Mathematical and Computational Applications

Article

Entropy Analysis for Hydromagnetic Darcy–Forchheimer Flow Subject to Soret and Dufour Effects

Sohail A. Khan * and Tasawar Hayat

Department of Mathematics, Quaid-I-Azam University, Islamabad 45320, Pakistan
* Correspondence: sohailahmadkhan93@gmail.com

Abstract: Here, our main aim is to examine the impacts of Dufour and Soret in a radiative Darcy–Forchheimer flow. Ohmic heating and the dissipative features are outlined. The characteristics of the thermo-diffusion and diffusion-thermo effects are addressed. A binary chemical reaction is deliberated. To examine the thermodynamical system performance, we discuss entropy generation. A non-linear differential system is computed by the finite difference technique. Variations in the velocity, concentration, thermal field and entropy rate for the emerging parameters are scrutinized. A decay in velocity is observed for the Forchheimer number. Higher estimation of the magnetic number has the opposite influence for the velocity and temperature. The velocity, concentration and thermal field have a similar effect on the suction variable. The temperature against the Dufour number is augmented. A decay in the concentration is found against the Soret number. A similar trend holds for the entropy rate through the radiation and diffusion variables. An augmentation in the entropy rate is observed for the diffusion variable.

Keywords: Darcy–Forchheimer model; thermal radiation; finite difference technique; viscous dissipation; Soret and Dufour impacts; chemical reaction; entropy generation

check for updates

Citation: Khan, S.A.; Hayat, T. Entropy Analysis for Hydromagnetic Darcy–Forchheimer Flow Subject to Soret and Dufour Effects. *Math. Comput. Appl.* **2022**, *27*, 80. https://doi.org/10.3390/mca27050080

Academic Editor: Zhuojia Fu

Received: 26 June 2022
Accepted: 14 September 2022
Published: 19 September 2022

1. Introduction

Henry Darcy established the framework of homogeneous liquid flow through a permeable medium throughout his work on the progression of water over saturated sand [1]. At higher flow rates, when inertial and boundary impacts arise, then the Darcy law cannot work appropriately. To overcome such an issue, Forchheimer gave the concept of the non-Darcy model through the insertion of a quadratic velocity term in a momentum expression [2]. Later on, the Forchheimer term was so named by Muskat [3]. The moment of fluid flowing through a permeable surface is of keen interest due to its significance in technical, biological and scientific fields such as artificial dialysis, gas turbines, atherosclerosis, catalytic converters, geo energy production and many others. Hayat et al. [4] explored the 2-D Darcy–Forchheimer flow of non-Newtonian liquid with variable properties. Pal and Mondal [5] addressed the convective flow of Darcy–Forchheimer liquid subject to a variable heat sink or source and viscosity. Non-uniform heat conductivity analysis in the reactive flow of Darcy–Forchheimer Carreau nanomaterial subject to a magnetic dipole was presented by Mallawi and Ullah [6]. Alshomrani and Ullah [7] studied the convective flow of Darcy–Forchheimer hybrid nanomaterial subject to a cubic autocatalysis chemical reaction. Seth and Mandal [8] discussed the hydromagnetic effect in rotating the flow of Darcy–Forchheimer Casson liquid toward a permeable space. Little analysis concerning a porous medium is discussed in [9–17].

Thermal and solutal transportation in a permeable surface has been a significant consideration of researchers during the last two decades. This is due to its usefulness in geothermal systems, catalytic reactors, nuclear waste repositories, areas of geosciences, chemical engineering, energy storage units, drying technology, heat insulation, heat exchangers for packed beds and many others. Initially, the Dufour effect in liquid was explored by Rastogi and Madan [18]. After that, the diffusion-thermo impact in a homogeneous mixture was investigated in [19,20]. Moorthy and Senthilvalivu [21] studied the Dufour and Soret outcomes in the convective flow of liquid of a non-uniform viscosity subject to a permeable medium. Non-uniform temperature in a convective fluid flow subject to thermal-diffusion and diffusion-thermo effects was illustrated by El-Arabawy [22]. Few reviews with reference to relevant titles have been discussed through certain studies [23–27]. The important reason for entropy production is the conversion of thermal energy in the occurrence of numerous examples of processes, such as fluid friction, kinetic energy, rotational moments, molecular resistance, the Joule Thomson effect, mass transport rate, and molecular vibration. The concept of entropy optimization in liquid flow was initially given by Bejan [28,29]. Entropy analysis in a water-based hybrid nanoliquid subject to mixed convection was discussed by Buonomo [30]. Irreversibility exploration in the dissipative flow of nanomaterial with melting and radiation over a stretching sheet was addressed by Khan et al. [31]. Some investigations of the entropy rate are mentioned in [32–39].

To our knowledge, no study has reported about entropy-optimized radiative Darcy–Forchheimer flows with Soret and Dufour features yet. A porous medium through a Darcy–Forchheimer relation is discussed. Dissipation, Ohmic heating and radiation are scrutinized in energy equations. The physical characteristics for the Soret and Dufour impacts are addressed. A first-order chemical reaction is deliberated. To examine the thermodynamical system performance, we discuss entropy optimization. Nonlinear differential systems are obtained through appropriate transformations. Non-dimensional differential systems are solved through the finite difference method. The performance of appropriate variables concerning the velocity, entropy generation, concentration and thermal field have been scrutinized.

2. Formulation

An unsteady radiative hydromagnetic Darcy–Forchheimer flow saturating a porous medium is discussed. Joule heating, viscous dissipation and thermal radiation in energy expression have been scrutinized. The Soret and Dufour effects are inspected. The impact of the entropy rate is addressed. Additionally, the flow is subject to a chemical reaction of the first order. A constant magnetic field with a strength (B_0) is applied. Consider $u = u_w = ax$ as the stretching velocity, with $a > 0$. The chosen magnetic Reynolds number is small. Figure 1 shows a flow sketch [31].

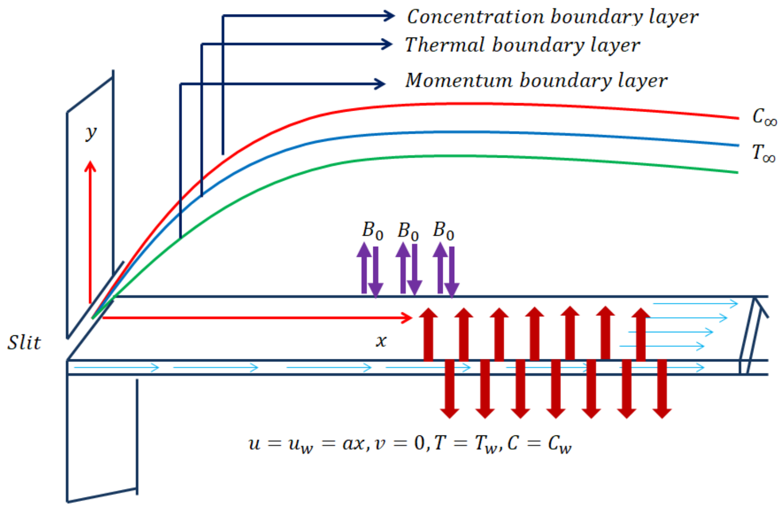

Figure 1. Flow sketch.

By taking into account the infinite plate, the term $\frac{\partial u}{\partial x}$ becomes zero. Here, the continuity equation becomes $\frac{\partial v}{\partial y} = 0$.

Under the above discussion, the related expression for constant suction becomes

$$v = -v_0 = \text{constant} \tag{1}$$

$$\frac{\partial u}{\partial t} - v_0\frac{\partial u}{\partial y} = \nu\frac{\partial^2 u}{\partial y^2} - \frac{\sigma B_0^2}{\rho}u - \frac{\nu}{k_p}u - Fu^2, \tag{2}$$

$$\left.\begin{array}{c} \frac{\partial T}{\partial t} - v_0\frac{\partial T}{\partial y} = \alpha\frac{\partial^2 T}{\partial y^2} + \frac{16}{3}\frac{\sigma^* T_\infty^3}{k^*(\rho c_p)}\frac{\partial^2 T}{\partial y^2} + \frac{\mu}{(\rho c_p)}(\frac{\partial u}{\partial y})^2 \\ +\frac{\sigma B_0^2}{(\rho c_p)}u^2 + \frac{D_B K_T}{C_s c_p}\frac{\partial^2 C}{\partial y^2} \end{array}\right\}, \tag{3}$$

$$\frac{\partial C}{\partial t} - v_0\frac{\partial C}{\partial y} = D_B\frac{\partial^2 C}{\partial y^2} + \frac{D_B K_T}{T_m}\frac{\partial^2 T}{\partial y^2} - k_r(C - C_\infty), \tag{4}$$

with

$$\left.\begin{array}{c} u = 0,\ T = T_\infty,\ C = C_\infty, \text{at } t = 0 \\ u = ax,\ T = T_w,\ C = C_w, \text{at } y = 0 \\ u \to 0,\ T \to T_\infty,\ C \to C_\infty,\ \text{as } y \to \infty \end{array}\right\}. \tag{5}$$

Consider the following formula:

$$\left.\begin{array}{c} \tau = \frac{v}{L_1^2}t,\ \xi = \frac{x}{L_1},\ \eta = \frac{y}{L_1},\ U(\tau,\eta) = \frac{L_1}{v}u, \\ \theta(\tau,\eta) = \frac{(T - T_\infty)}{(T_w - T_\infty)},\ \phi(\tau,\eta) = \frac{C - C_\infty}{C_w - C_\infty}, \end{array}\right\}, \tag{6}$$

Then, we have

$$\frac{\partial U}{\partial \tau} - S\frac{\partial U}{\partial \eta} = \frac{\partial^2 U}{\partial \eta^2} - MU - \lambda U - FrU^2, \tag{7}$$

$$\frac{\partial \theta}{\partial \tau} - S\frac{\partial \theta}{\partial \eta} = \frac{1}{\Pr}(1 + Rd)\frac{\partial^2 \theta}{\partial \eta^2} + Ec(\frac{\partial U}{\partial \eta})^2 + MEcU^2 + Du\frac{\partial^2 \phi}{\partial \eta^2}, \tag{8}$$

$$\frac{\partial \phi}{\partial \tau} - S\frac{\partial \phi}{\partial \eta} = \frac{1}{Sc}\frac{\partial^2 \phi}{\partial \eta^2} + Sr\frac{\partial^2 \theta}{\partial \eta^2} - \gamma\phi, \tag{9}$$

with

$$\left.\begin{array}{c} U = 0,\ \theta = 0,\ \phi = 0,\ \text{at } \tau = 0 \\ U = \xi\,\mathrm{Re},\ \theta = 1, \phi = 1,\ \text{at } \eta = 0 \\ U \to 0,\ \theta \to 0,\ \phi \to 0,\ \text{as } \eta \to \infty \end{array}\right\} \tag{10}$$

Here the non-dimensional variables are $S(=\frac{v_0}{\nu}L_1)$, $M\left(=\frac{\sigma B_o^2 L_1^2}{\nu\rho}\right)$, $\mathrm{Re}\left(=\frac{aL_1^2}{\nu}\right)$, $Sr\left(=\frac{DK_T(T_w - T_\infty)}{\nu T_m(C_w - C_\infty)}\right)$, $F_r\left(=\frac{C_b}{\sqrt{k_p}}L_1\right)$, $\Pr(=\frac{\nu}{\alpha})$, $\lambda\left(=\frac{L_1^2}{k_p}\right)$, $E_C\left(=\frac{\nu^2}{c_p L_1^2(T_w - T_\infty)}\right)$, $\gamma\left(=\frac{k_r L_1^2}{\nu}\right)$, $Du\left(=\frac{D_B K_T(C_w - C_\infty)}{\nu C_s c_p(T_w - T_\infty)}\right)$, $Rd\left(=\frac{16\sigma^* T_\infty^3}{3k^* k}\right)$, $Sc\left(=\frac{\nu}{D_B}\right)$ and $Br(=\Pr Ec)$.

3. Engineering Contents of Interest

3.1. Nusselt Number

Here, we have

$$Nu_x = \frac{xq_w}{k(T_w - T_\infty)}, \tag{11}$$

with the heat flux q_w given by

$$q_w = -\left(k + \frac{16\sigma^* T_\infty^3}{3k^*}\right)\left(\frac{\partial T}{\partial y}\right)\Big|_{y=0} \tag{12}$$

We finally have

$$Nu_x = -\xi(1+Rd)\left(\frac{\partial\theta}{\partial\eta}\right)_{\eta=0}. \tag{13}$$

3.2. Sherwood Number

This is given as

$$Sh_x = \frac{xj_w}{D_B(C_w - C_\infty)}, \tag{14}$$

in which the mass flux j_w is defined as

$$j_w = -D_B(\frac{\partial C}{\partial y})\Big|_{y=0}, \tag{15}$$

We can write

$$Sh_x = -\xi(\frac{\partial\phi}{\partial\eta})_{\eta=0}. \tag{16}$$

4. Entropy

The important reason for entropy production is the conversion of thermal energy in the occurrence of numerous processes, such as fluid friction, kinetic energy, rotational moment, molecular resistance, the Joule–Thomson effect, mass transport rate and molecular vibration. We have the following [30–33]:

$$\left.\begin{array}{c} S_G = \frac{k}{T_\infty^2}\left(1+\frac{16\sigma^* T_\infty^3}{3k^*k}\right)\left(\frac{\partial T}{\partial y}\right)^2 + \frac{\mu_f}{T_\infty}\left(\frac{\partial u}{\partial y}\right)^2 + \frac{\mu}{k_p T_\infty}u^2 \\ +\frac{\sigma B_o^2}{T_\infty}u^2 + \frac{RD_B}{T_\infty}\left(\frac{\partial T}{\partial y}\frac{\partial C}{\partial y}\right) + \frac{RD_B}{C_\infty}\left(\frac{\partial C}{\partial y}\right)^2 \end{array}\right\}, \tag{17}$$

The dimensionless expression is

$$\left.\begin{array}{c} N_G(\tau,\eta) = \alpha_1(1+Rd)\left(\frac{\partial\theta}{\partial\eta}\right)^2 + Br\left(\frac{\partial U}{\partial\eta}\right)^2 + Br\lambda U^2 \\ +MBrU^2 + L\left(\frac{\partial\theta}{\partial\eta}\frac{\partial\phi}{\partial\eta}\right) + L\frac{\alpha_2}{\alpha_1}\left(\frac{\partial\phi}{\partial\eta}\right)^2 \end{array}\right\} \tag{18}$$

In the above expression, the dimensionless parameters are $\alpha_1\left(=\frac{(T_w-T_\infty)}{T_\infty}\right)$, $N_G\left(=\frac{S_G T_\infty L_1^2}{k(T_w-T_\infty)}\right)$, $L\left(=\frac{RD_B(C_w-C_\infty)}{k}\right)$ and $\alpha_2\left(=\frac{(C_w-C_\infty)}{C_\infty}\right)$.

5. Solution Methodology

Using the finite difference method, we can solve the nonlinear differential system [40–43] by writing

$$\left.\begin{array}{c} \frac{\partial U}{\partial\tau} = \frac{U_a^{n+1}-U_a^n}{\Delta\tau}, \frac{\partial U}{\partial\eta} = \frac{U_{a+1}^n - U_a^n}{\Delta\eta} \\ \frac{\partial\theta}{\partial\tau} = \frac{\theta_a^{n+1}-\theta_s^k}{\Delta\tau}, \frac{\partial\theta}{\partial\eta} = \frac{\theta_{a+1}^n-\theta_a^n}{\Delta\eta} \\ \frac{\partial\phi}{\partial\tau} = \frac{\phi_a^{n+1}-\phi_a^n}{\Delta\tau}, \frac{\partial\phi}{\partial\eta} = \frac{\phi_{a+1}^n-\phi_a^n}{\Delta\eta} \\ \frac{\partial^2 U}{\partial\eta^2} = \frac{U_{a+1}^n - 2U_a^n + U_{a-1}^n}{(\Delta\eta)^2}, \frac{\partial^2\theta}{\partial\eta^2} = \frac{\theta_{a+1}^n-2\theta_a^n+\theta_{a-1}^n}{(\Delta\eta)^2} \\ \frac{\partial^2\phi}{\partial\eta^2} = \frac{\phi_{a+1}^n - 2\phi_a^n + \phi_{a-1}^n}{(\Delta\eta)^2} \end{array}\right\}, \tag{19}$$

By employing Equation (23) in Equations (8)–(10), we obtain

$$\frac{U_a^{n+1}-U_a^n}{\Delta\tau} - S\frac{U_{a+1}^n - U_a^n}{\Delta\eta} = \frac{U_{a+1}^n - 2U_a^n + U_{a-1}^n}{(\Delta\eta)^2} - MU_a^n - \lambda U_a^n - Fr(U_a^n)^2, \tag{20}$$

$$\left.\begin{array}{r}\frac{\theta_a^{n+1}-\theta_a^n}{\Delta\tau}-S\frac{\theta_{a+1}^n-\theta_a^n}{\Delta\eta}=\frac{(1+Rd)}{P_r}\frac{\theta_{a+1}^n-2\theta_a^n+\theta_{a-1}^n}{(\Delta\eta)^2}+Ec\left(\frac{U_{a+1}^n-U_a^n}{\Delta\eta}\right)^2\\ +MEc(U_a^n)^2+Du\left(\frac{\phi_{a+1}^n-2\phi_a^n+\phi_{a-1}^n}{(\Delta\eta)^2}\right)\end{array}\right\} \tag{21}$$

$$\frac{\phi_a^{n+1}-\phi_a^n}{\Delta\tau}-S\frac{\phi_{a+1}^n-\phi_a^n}{\Delta\eta}=\frac{1}{Sc}\frac{\phi_{a+1}^n-2\phi_a^n+\phi_{a-1}^n}{(\Delta\eta)^2}+Sr\frac{\theta_{a+1}^n-2\theta_a^n+\theta_{a-1}^n}{(\Delta\eta)^2}-\gamma\phi_a^n, \tag{22}$$

with

$$\left.\begin{array}{r}U_a^0=0,\ \theta_a^0=0,\ \phi_a^0=0,\\ U_0^n=1,\ \theta_0^n=1,\ \phi_0^n=1,\\ U_\infty^n\to 0,\ \theta_\infty^n\to 0,\ \phi_\infty^n\to 0\end{array}\right\} \tag{23}$$

The entropy generation expression yields

$$\left.\begin{array}{r}N_G(\tau,\xi,\eta)=\alpha_1(1+Rd)(\frac{\theta_{a+1}^n-\theta_a^n}{\Delta\eta})^2+Br\left(\frac{U_{a+1}^n-U_a^n}{\Delta\eta}\right)^2+Br\lambda(U_a^n)^2\\ +MBr(U_a^n)^2+L(\frac{\theta_{a+1}^n-\theta_a^n}{\Delta\eta}.\frac{\phi_{a+1}^n-\phi_a^n}{\Delta\eta})+L\frac{\alpha_2}{\alpha_1}(\frac{\phi_{a+1}^n-\phi_a^n}{\Delta\eta})^2\end{array}\right\} \tag{24}$$

6. Graphical Results and Review

The physical interpretation of the parameters of the concentration, entropy rate, velocity and temperature have been investigated. The present observations are compared with previous published results in Table 1, and excellent agreement is noticed.

Table 1. Comparison of Nusselt numbers with [44].

Pr	Bidin and Nazar [44]	Recent Outcomes
1.0	0.9547	0.954710
2.0	1.4714	1.471409
3.0	1.8961	1.896115

6.1. Velocity

The influence of suction (S) upon the velocity $(U(\tau,\eta))$ is sketched in Figure 2. Obviously, a higher estimation of the suction parameter (S) decays the velocity. As expected, this is in accordance to the physical facts. Figure 3 displays the velocity against a magnetic field. Actually, reduction occurs in the velocity for (M). A physically higher (M) value corresponds to amplifying the Lorentz force which the flow opposes. Hence, velocity decay is guaranteed. Figure 4 was developed in order to recognize the velocity $(U(\tau,\eta))$ design with variation in the Forchheimer number (Fr). A larger estimation for the Forchheimer number decays the velocity $(U(\tau,\eta))$. The influence of (λ) on $(U(\tau,\eta))$ is illustrated in Figure 5. Clearly, $U(\tau,\eta)$ decays against higher λ values.

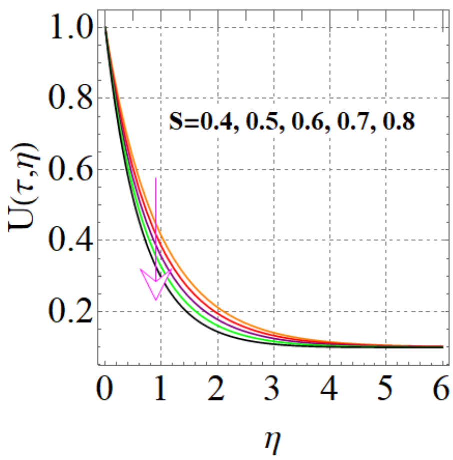

Figure 2. $U(\tau,\eta)$ via S.

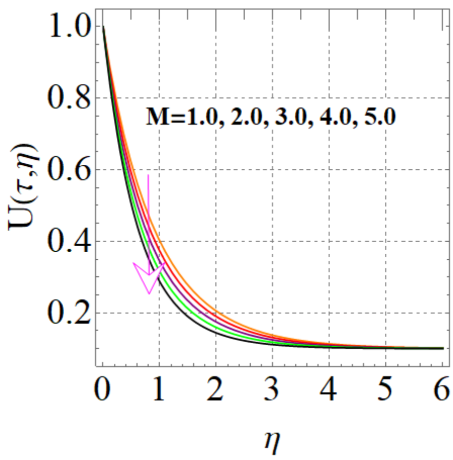

Figure 3. $U(\tau,\eta)$ via M.

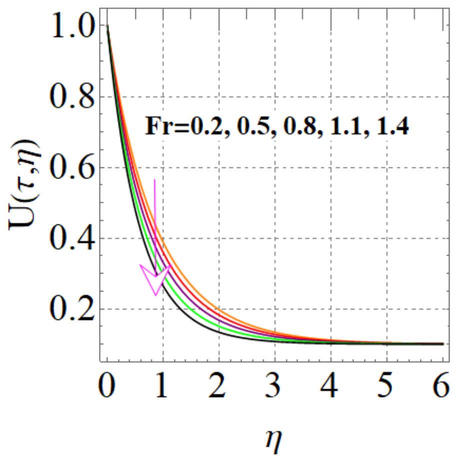

Figure 4. $U(\tau,\eta)$ via Fr.

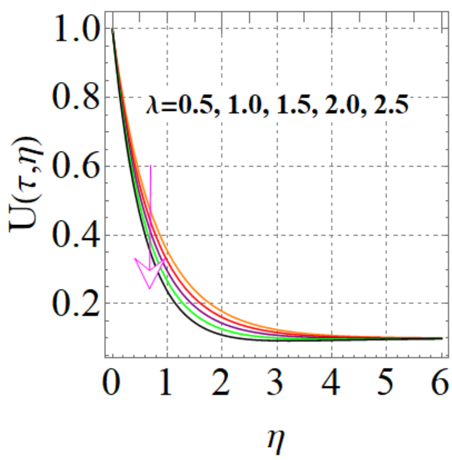

Figure 5. $U(\tau,\eta)$ via λ.

6.2. Temperature

Figures 6 and 7 are for the thermal field against the suction and magnetic variables (S and M). A similar scenario holds for the thermal field ($\theta(\tau,\eta)$) through the suction and magnetic variables. Figure 8 portrays the performance of the radiation against the temperature ($\theta(\tau,\eta)$). Larger radiation values lead to the temperature ($\theta(\tau,\eta)$) increasing. Figure 9 displays the performance of the thermal field against the Prandtl number. A larger approximation of (Pr) corresponds to the decay of the thermal diffusivity, and consequently, the temperature ($\theta(\tau,\eta)$) decreases. Figure 10 displays the impact of the thermal field $\theta(\tau, \eta)$ on the Eckert number (Ec). A higher estimation for (Ec) corresponds to the temperature being higher.

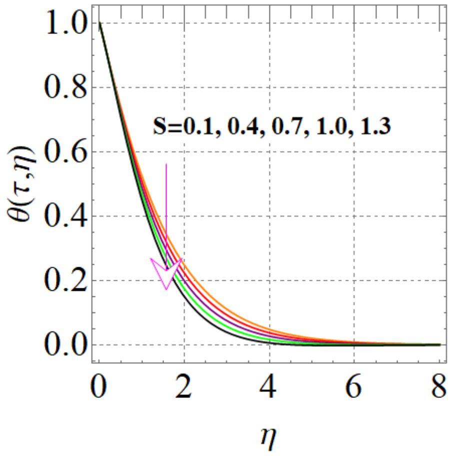

Figure 6. $\theta(\tau, \eta)$ via S.

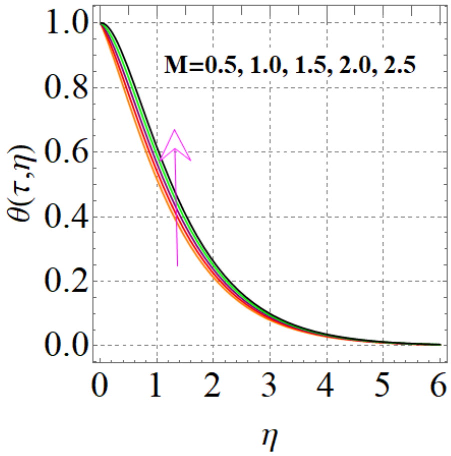

Figure 7. $\theta(\tau, \eta)$ via M.

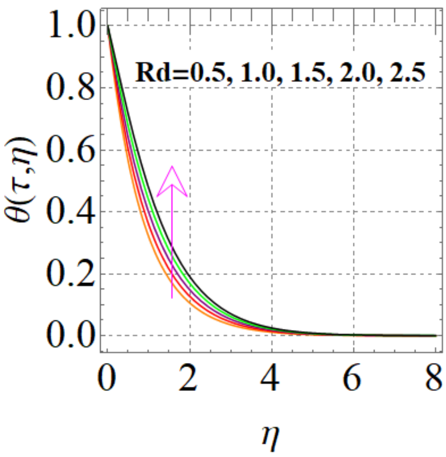

Figure 8. $\theta(\tau, \eta)$ via Rd.

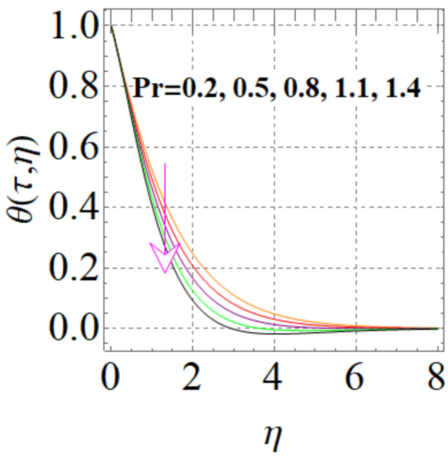

Figure 9. $\theta(\tau,\eta)$ via Pr.

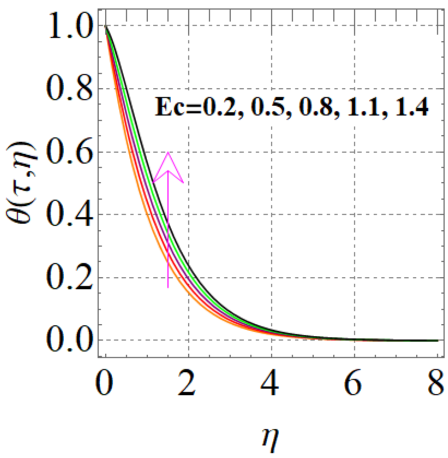

Figure 10. $\theta(\tau,\eta)$ via Ec.

6.3. Concentration

Figure 11 exhibits the concentration performance against the suction variable (S). Clearly, the concentration ($\phi(\tau,\eta)$) was reduced against larger (S) values. Figure 12 shows the performance of the concentration ($\phi(\tau,\eta)$) versus (Sc). An increment (Sc) decayed the mass diffusivity, and thus the concentration ($\phi(\tau,\eta)$) diminished. An amplification of the Soret number (Sr) led to a decaying value for $\phi(\tau,\eta)$ (see Figure 13). Figure 14 comprises the impact of $\phi(\tau,\eta)$ on γ. Here, $\phi(\tau,\eta)$ decreased against γ.

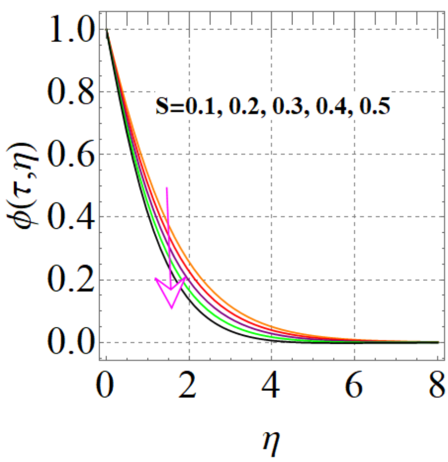

Figure 11. $\phi(\tau,\eta)$ via S.

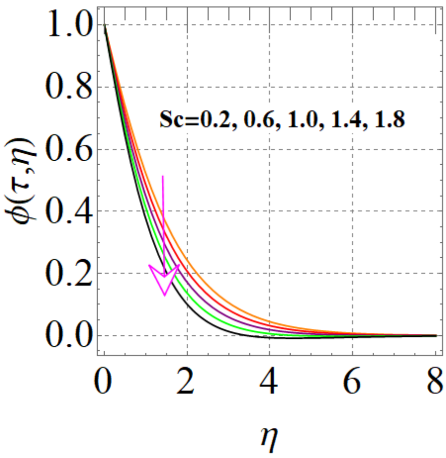

Figure 12. $\phi(\tau, \eta)$ via Sc.

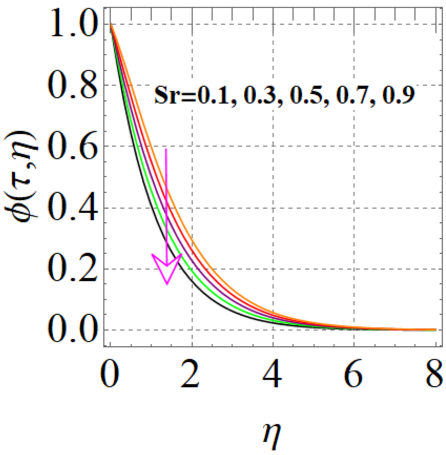

Figure 13. $\phi(\tau, \eta)$ via Sr.

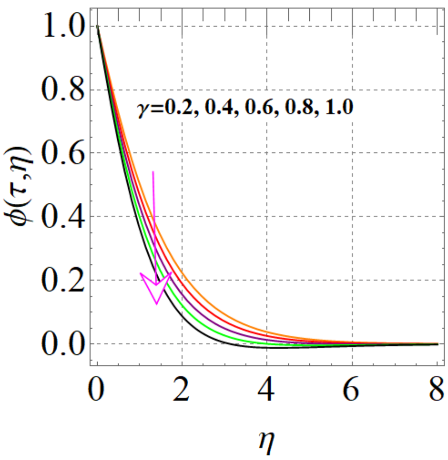

Figure 14. $\phi(\tau, \eta)$ via γ.

6.4. Entropy Generation Rate

The influence of the entropy rate ($N_G(\tau, \eta)$) via the radiation variable is disclosed in Figure 15. Clearly, a greater Rd value improved the radiation emission, which boosted the collision between the fluid particles, and so $N_G(\tau, \eta)$ was enhanced. Figure 16 discloses the impact of L on $N_G(\tau, \eta)$. As predicted, the entropy generation ($S_G(\eta)$) was greater via the higher approximation of L. A larger approximation of the Brinkman (Br) number enhanced the entropy generation ($S_G(\eta)$) (see Figure 17). This is because of augmentation through a higher Br value causing the viscous features to improve. As a result, the entropy rate rose. Figure 18 demonstrates the entropy rate for the magnetic parameter. A larger approximation of the magnetic variable led to an increase in the entropy rate.

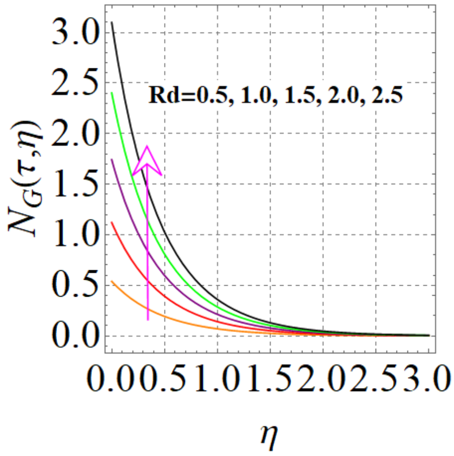

Figure 15. $N_G(\tau,\eta)$ via Rd.

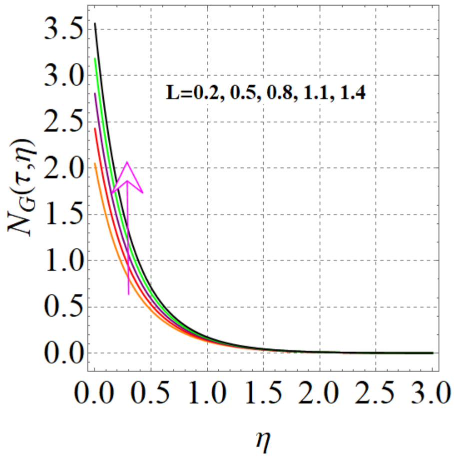

Figure 16. $N_G(\tau,\eta)$ via L.

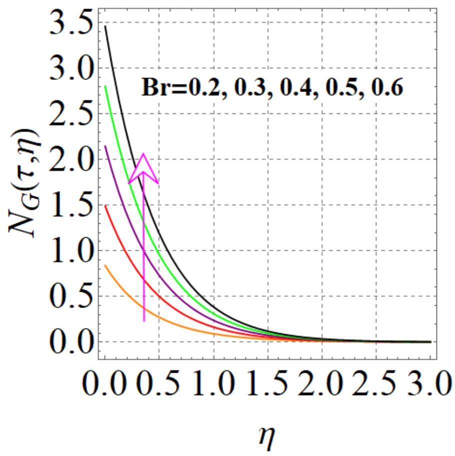

Figure 17. $N_G(\tau,\eta)$ via Br.

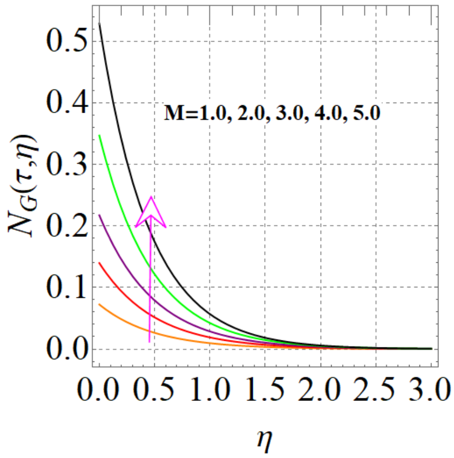

Figure 18. $N_G(\tau, \eta)$ via M.

7. Closing Points

- The theermal field and velocity for the magnetic field had opposing trends.
- A decrease in velocity was noted for the Forchheimer number and suction variable.
- The velocity versus the porosity parameter was decreased.
- Similar behavior for the concentration and temperature against suction was noticed.
- The temperatures for the Eckert and Prandtl numbers were dissimilar.
- Radiation for the entropy and temperature had a similar role.
- The concentration decayed via larger approximation of the Soret number and reaction parameter.
- A decay in concentration against the Schmidt number held.
- Entropy generation enhancement against the Brinkman number and diffusion variable was noticed.
- The entropy rate was boosted with variation in the diffusion variable.

Author Contributions: Conceptualization, S.A.K. and T.H.; Formal analysis, S.A.K. and T.H.; Investigation, S.A.K. and T.H.; Methodology, S.A.K. and T.H.; Supervision, T.H.; Writing—original draft, S.A.K.; Writing—review & editing, S.A.K. All authors have read and agreed to the published version of the manuscript.

Funding: This research received no external funding.

Conflicts of Interest: The authors declare no conflict of interest.

Nomenclature

u, v	Velocity components (ms^{-1})	x, y	Cartesian coordinates (m)
t	Time (s)	$v_0 > 0$	Suction velocity (ms^{-1})
ρ	Density (kgm^{-3})	σ	Electrical conductivity (Sm^{-1})
T	Temperature (K)	c_p	Specific heat (Jkg^{-1}K^{-1})
k_p	Porous medium permeability (m^2)	C_b	Drag coefficient
T_w	Wall temperature (K)	α	Thermal diffusivity (m^2 s^{-1})
k	Thermal conductivity (Wm^{-1}K^{-1})	T_∞	Ambient temperature (K)
σ^*	Stefan–Boltzman constant (Wm^{-2}K^{-4})	K_T	Thermal diffusion ratio
C_s	Concentration susceptibility	k^*	Mean absorption coefficient (cm^{-1})
C	Concentration	k_r	Reaction rate (s)
C_w	Wall concentration	D_B	Mass diffusivity (m^2 s^{-1})
L_1	Reference length (m)	C_∞	Ambient concentration
u_w	Stretching velocity (ms^{-1})	a	Stretching rate constant (s^{-1})
Nu_x	Nusselt number	q_w	Heat flux (Wm^2)

Sh_x	Sherwood number	j_w	Mass flux
R	Molar gas constant ($\mathrm{kgm^2\,s^{-2}K^{-1}mol^{-1}}$)	M	Magnetic variable
λ	Porosity variable	Fr	Forchheimer number
S	Suction parameter	Pr	Prandtl number
Rd	Radiation variable	Du	Dufour number
Ec	Eckert number	γ	Reaction variable
Sr	Soret number	Re	Reynold number
Sc	Schmidt number	N_G	Entropy rate
α_1	Temperature ratio variable	Br	Brinkman number
α_2	Concentration ratio variable	L	Diffusion variable
T_m	Mean fluid temperature (K)	B_0	Magnetic field strength

References

1. Darcy, H. *Les Fontaines Publiques de la Ville dr Dijion*; Dalmont, V., Ed.; Typ. Hennuyer: Paris, France, 1856; pp. 647–658.
2. Forchheimer, P. Wasserbewegung durch boden. *Z. Vereins Dtsch. Ingenieure* **1901**, *45*, 1782–1788.
3. Muskat, M. *The Flow of Homogeneous Fluids through Porous Media*; JW Edwards, Inc.: Ann Arbor, MI, USA, 1946.
4. Hayat, T.; Muhammad, T.; Al-Mezal, S.; Liao, S.J. Darcy-Forchheimer flow with variable thermal conductivity and Cattaneo-Christov heat flux. *Int. J. Numer. Methods Heat Fluid Flow* **2016**, *26*, 2355–2369. [CrossRef]
5. Pal, D.; Mondal, H. Hydromagnetic convective diffusion of species in Darcy-Forchheimer porous medium with non-uniform heat source/sink and variable viscosity. *Int. Commun. Heat Mass Transf.* **2012**, *39*, 913–917. [CrossRef]
6. Mallawi, F.; Ullah, M.Z. Conductivity and energy change in Carreau nanofluid flow along with magnetic dipole and Darcy-Forchheimer relation. *Alex. Eng. J.* **2021**, *60*, 3565–3575. [CrossRef]
7. Alshomrani, A.S.; Ullah, M.Z. Effects of homogeneous-heterogeneous reactions and convective condition in Darcy-Forchheimer flow of carbon nanotubes. *J. Heat Transf.* **2019**, *141*, 012405. [CrossRef]
8. Seth, G.S.; Mandal, P.K. Hydromagnetic rotating flow of Casson fluid in Darcy-Forchheimer porous medium. *MATEC Web Conf.* **2018**, *192*, 02059. [CrossRef]
9. Khan, S.A.; Hayat, T.; Alsaedi, A. Irreversibility analysis in Darcy-Forchheimer flow of viscous fluid with Dufour and Soret effects via finite difference method. *Case Stud. Therm. Eng.* **2021**, *26*, 101065. [CrossRef]
10. Azam, M.; Xu, T.; Khan, M. Numerical simulation for variable thermal properties and heat source/sink in flow of Cross nanofluid over a moving cylinder. *Int. Commun. Heat Mass Transf.* **2020**, *118*, 104832. [CrossRef]
11. Wu, Y.; Kou, J.; Sun, S. Matrix acidization in fractured porous media with the continuum fracture model and thermal Darcy-Brinkman-Forchheimer framework. *J. Pet. Sci. Eng.* **2022**, *211*, 110210. [CrossRef]
12. Haider, F.; Hayat, T.; Alsaedi, A. Flow of hybrid nanofluid through Darcy-Forchheimer porous space with variable characteristics. *Alex. Eng. J.* **2021**, *60*, 3047–3056. [CrossRef]
13. Tayyab, M.; Siddique, I.; Jarad, F.; Ashraf, M.A.; Ali, B. Numerical solution of 3D rotating nanofluid flow subject to Darcy-Forchheimer law, bio-convection and activation energy. *S. Afr. J. Chem. Eng.* **2022**, *40*, 48–56. [CrossRef]
14. Nawaz, M.; Sadiq, M.A. Unsteady heat transfer enhancement in Williamson fluid in Darcy-Forchheimer porous medium under non-Fourier condition of heat flux. *Case Stud. Therm. Eng.* **2021**, *28*, 101647. [CrossRef]
15. Ali, L.; Wang, Y.; Ali, B.; Liu, X.; Din, A.; Mdallal, Q.A. The function of nanoparticle's diameter and Darcy-Forchheimer flow over a cylinder with effect of magnetic field and thermal radiation. *Case Stud. Therm. Eng.* **2021**, *28*, 101392. [CrossRef]
16. Bejawada, S.G.; Reddy, Y.D.; Jamshed, W.; Eid, M.R.; Safdar, R.; Nisar, K.S.; Isa, S.S.P.M.; Alam, M.M.; Parvin, S. 2D mixed convection non-Darcy model with radiation effect in a nanofluid over an inclined wavy surface. *Alex. Eng. J.* **2022**, *61*, 9965–9976. [CrossRef]
17. Eid, M.R.; Mahny, K.L.; Al-Hossainy, A.F. Homogeneous-heterogeneous catalysis on electromagnetic radiative Prandtl fluid flow: Darcy-Forchheimer substance scheme. *Surf. Interfaces* **2021**, *24*, 101119. [CrossRef]
18. Rastogi, R.P.; Madan, G.L. Dufour Effect in Liquids. *J. Chem. Phys.* **1965**, *43*, 4179–4180. [CrossRef]
19. Rastogi, R.P.; Nigam, R.K. Cross-phenomenological coefficients. Part 6—Dufour effect in gases. *Trans. Faraday Soc.* **1966**, *62*, 3325–3330. [CrossRef]
20. Rastogi, R.P.; Yadava, B.L.S. Dufour effect in liquid mixtures. *J. Chem. Phys.* **1969**, *51*, 2826–2830. [CrossRef]
21. Moorthy, M.B.K.; Senthilvadivu, K. Soret and Dufour effects on natural convection flow past a vertical surface in a porous medium with variable viscosity. *J. Math. Phys.* **2012**, *2012*, 634806. [CrossRef]
22. El-Arabawy, H.A.M. Soret and dufour effects on natural convection flow past a vertical surface in a porous medium with variable surface temperature. *J. Math. Stat.* **2009**, *5*, 190–198. [CrossRef]
23. Reddy, G.J.; Raju, R.S.; Manideep, C.; Rao, J.A. Thermal diffusion and diffusion thermo effects on unsteady MHD fluid flow past a moving vertical plate embedded in porous medium in the presence of Hall current and rotating system. *Trans. A. Razmadze Math. Inst.* **2016**, *170*, 243–265. [CrossRef]

24. Dursunkaya, Z.; Worek, W.M. Diffusion-thermo and thermal-diffusion effects in transient and steady natural convection from vertical surface. *Int. J. Heat Mass Transf.* **1992**, *35*, 2060–2067. [CrossRef]
25. Khan, S.A.; Hayat, T.; Khan, M.I.; Alsaedi, A. Salient features of Dufour and Soret effect in radiative MHD flow of viscous fluid by a rotating cone with entropy generation. *Int. J. Hydrogen Energy* **2020**, *45*, 4552–14564. [CrossRef]
26. Bekezhanova, V.B.; Goncharova, O.N. Influence of the Dufour and Soret effects on the characteristics of evaporating liquid flows. *Int. J. Heat Mass Transf.* **2020**, *154*, 119696. [CrossRef]
27. Jiang, N.; Studer, E.; Podvin, B. Physical modeling of simultaneous heat and mass transfer: Species interdiffusion, Soret effect and Dufour effect. *Int. J. Heat Mass Transf.* **2020**, *156*, 119758. [CrossRef]
28. Bejan, A. Second law analysis in heat transfer. *Energy Int. J.* **1980**, *5*, 721–732. [CrossRef]
29. Bejan, A. *Entropy Generation Minimization*; CRC Press: New York, NY, USA, 1996.
30. Buonomo, B.; Pasqua, A.; Manca, O.; Nappo, S.; Nardini, S. Entropy generation analysis of laminar forced convection with nanofluids at pore length scale in porous structures with Kelvin cells. *Int. Commun. Heat Mass Transf.* **2022**, *132*, 105883. [CrossRef]
31. Khan, S.A.; Hayat, T.; Alsaedi, A.; Ahmad, B. Melting heat transportation in radiative flow of nanomaterials with irreversibility analysis. *Renew. Sustain. Energy Rev.* **2021**, *140*, 110739. [CrossRef]
32. Tayebi, T.; Öztop, H.F.; Chamkha, A.J. Natural convection and entropy production in hybrid nanofluid filled-annular elliptical cavity with internal heat generation or absorption. *Therm. Sci. Eng. Prog.* **2020**, *19*, 100605. [CrossRef]
33. Abbas, Z.; Naveed, M.; Hussain, M.; Salamat, N. Analysis of entropy generation for MHD flow of viscous fluid embedded in a vertical porous channel with thermal radiation. *Alex. Eng. J.* **2020**, *59*, 3395–3405. [CrossRef]
34. Rahmanian, S.; Koushkaki, H.R.; Shahsavar, A. Numerical assessment on the hydrothermal behaviour and entropy generation characteristics of boehmite alumina nanofluid flow through a concentrating photovoltaic/thermal system considering various shapes for nanoparticle. *Sustain. Energy Technol. Assess.* **2022**, *52*, 102143. [CrossRef]
35. Nayak, M.K.; Mabood, F.; Dogonchi, A.S.; Khan, W.A. Electromagnetic flow of SWCNT/MWCNT suspensions with optimized entropy generation and cubic auto catalysis chemical reaction. *Int. Commun. Heat Mass Transf.* **2020**, *2020*, 104996. [CrossRef]
36. Kumawat, C.; Sharma, B.K.; Al-Mdallal, Q.M.; Gorji, M.R. Entropy generation for MHD two phase blood flow through a curved permeable artery having variable viscosity with heat and mass transfer. *Int. Commun. Heat Mass Transf.* **2022**, *133*, 105954. [CrossRef]
37. Liu, Y.; Jian, Y.; Tan, W. Entropy generation of electromagnetohydrodynamic (EMHD) flow in a curved rectangular microchannel. *Int. J. Heat Mass Transf.* **2018**, *127*, 901–913. [CrossRef]
38. Alotaibi, H.; Eid, M.R. Thermal analysis of 3D electromagnetic radiative nanofluid flow with suction/blowing: Darcy–Forchheimer scheme. *Micromachines* **2021**, *12*, 1395. [CrossRef]
39. Eid, M.R.; Mabood, F. Entropy analysis of a hydromagnetic micropolar dusty carbon NTs-kerosene nanofluid with heat generation: Darcy–Forchheimer scheme. *J. Therm. Anal. Calorim.* **2021**, *143*, 2419–2436. [CrossRef]
40. Swain, I.; Pattanayak, H.; Das, M.; Singh, T. Finite difference solution of free convective heat transfer of non-Newtonian power law fluids from a vertical plate. *Glob. J. Pure Appl. Math.* **2015**, *11*, 339–348.
41. Adekanye, O.; Washington, T. Nonstandard finite difference scheme for a Tacoma narrows bridge model. *Appl. Math. Model.* **2018**, *62*, 223–236. [CrossRef]
42. Hayat, T.; Ullah, H.; Ahmad, B.; Alhodaly, M.S. Heat transfer analysis in convective flow of Jeffrey nanofluid by vertical stretchable cylinder. *Int. Commun. Heat Mass Transf.* **2021**, *120*, 104965. [CrossRef]
43. Khan, Z.H.; Makinde, O.D.; Ahmad, R.; Khan, W.A. Numerical study of unsteady MHD flow and entropy generation in a rotating permeable channel with slip and Hall effects. *Commun. Theor. Phys.* **2018**, *70*, 641–650. [CrossRef]
44. Bidin, B.; Nazar, R. Numerical solution of the boundary layer flow over an exponentially stretching sheet with thermal radiation. *Eur. J. Sci. Res.* **2009**, *33*, 710–717.